JACS
JOURNAL OF THE AMERICAN CHEMICAL SOCIETY
Article
pubs.acs.org/JACS

Hydrogen Sulfide Oxidation by Myoglobin

Trever Bostelaar,[†,#] Victor Vitvitsky,[†,#] Jacques Kumutima,[‡] Brianne E. Lewis,[§] Pramod K. Yadav,[†] Thomas C. Brunold,[∥] Milos Filipovic,[⊥] Nicolai Lehnert,[‡] Timothy L. Stemmler,[§] and Ruma Banerjee*[,†]

[†]Department of Biological Chemistry and [‡]Department of Chemistry and Department of Biophysics, University of Michigan, Ann Arbor, Michigan 48109, United States

[§]Department of Pharmaceutical Science, Wayne State University, Detroit, Michigan 48201-2417, United States

[∥]Department of Chemistry, University of Wisconsin, Madison, Wisconsin 53706, United States

[⊥]University of Bordeaux, IBGC, and CNRS, IBGC, UMR 5095, F-33077 Bordeaux, France

ABSTRACT: Enzymes in the sulfur network generate the signaling molecule, hydrogen sulfide (H_2S), from the amino acids cysteine and homocysteine. Since it is toxic at elevated concentrations, cells are equipped to clear H_2S. A canonical sulfide oxidation pathway operates in mitochondria, converting H_2S to thiosulfate and sulfate. We have recently discovered the ability of ferric hemoglobin to oxidize sulfide to thiosulfate and iron-bound hydropolysulfides. In this study, we report that myoglobin exhibits a similar capacity for sulfide oxidation. We have trapped and characterized iron-bound sulfur intermediates using cryo-mass spectrometry and X-ray absorption spectroscopy. Further support for the postulated intermediates in the chemically challenging conversion of H_2S to thiosulfate and iron-bound catenated sulfur products is provided by EPR and resonance Raman spectroscopy in addition to density functional theory computational results. We speculate that the unusual sensitivity of skeletal muscle cytochrome c oxidase to sulfide poisoning in ethylmalonic encephalopathy, resulting from the deficiency in a mitochondrial sulfide oxidation enzyme, might be due to the concentration of H_2S by myoglobin in this tissue.

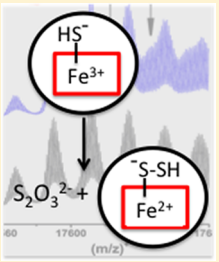

INTRODUCTION

Hydrogen sulfide (H_2S) is a signaling molecule at low concentrations[1,2] but is toxic at high concentrations, choking aerobic respiration by targeting the heme and copper centers in cytochrome c oxidase.[3] Enzymes in the sulfur metabolic network are responsible for H_2S biogenesis, while a mitochondrial resident pathway is responsible for its oxidative destruction.[4] The mechanism by which H_2S signals is under active investigation. Persulfidation, a posttranslational modification of cysteines, has emerged as a major transducer of H_2S signals.[5,6] A less well-studied aspect of sulfide biochemistry is the potential of H_2S to interact with metal centers. The interaction between sulfide and heme iron is very important in organisms that live in sulfide-rich environments and have specialized hemoglobins for binding and conveying H_2S to symbiotic bacteria that extract energy from sulfide oxidation. The reaction of H_2S with hemoglobin and myoglobin to produce sulfheme derivatives has been extensively investigated and results in the covalent addition of sulfide to one of the pyrrole rings.[7] Sulfheme formation has also been noted during the catalytic cycle of lactoperoxidase[8] and catalase.[9]

More recently, we have described a new chemical interaction between ferric hemoglobin (Fe^{III}−Hb) and H_2S that leads to catalytic turnover of sulfide.[10] The products of this heme-dependent sulfide oxidation are thiosulfate and iron-bound hydropolysulfides. The bimolecular rate constant for binding of sulfide to Fe^{III}−Hb is 3.2×10^3 M^{-1} s^{-1} at pH 7.4 (37 °C) and is inversely proportional to pH. The presence of the H_2S generating enzyme 3-mercaptopyruvate sulfurtransferase in red blood cells, together with the absence of mitochondria that house the canonical sulfide oxidation machinery, suggests that Fe^{III}−Hb-dependent oxidation of H_2S might be physiologically important for H_2S homeostasis in the circulatory system.[10] In other cell types that have mitochondria, the combined action of four enzymes converts H_2S to thiosulfate and sulfate.[1,11] The electrons released from sulfide oxidation in the first step in this pathway are funneled to the electron transport chain at the level of complex III.[12]

Myoglobin, like hemoglobin, is a globular hemeprotein designed to bind oxygen to ferrous iron. The first structural insights into sperm whale myoglobin were provided by the crystal structure of this monomeric protein solved by Kendrew and co-workers in 1958.[13] In addition to its well-studied role as an O_2 storehouse in skeletal and heart muscle, other functions for myoglobin have emerged from studies on myoglobin knockout mice that, surprisingly, are viable.[14] Myoglobin appears to also play a role in NO• homeostasis.[15−18] Under normoxic conditions, both deoxy- (Fe^{II}-Mb) and oxy-myoglobin (Fe^{II}-O_2-Mb) react rapidly with NO•, another gaseous signaling molecule, with a bimolecular rate constant of ∼(2−3) × 10^7 M^{-1} s^{-1} (20 °C, pH 7.0). While binding of NO• to Fe^{II}-Mb is reversible, binding to Fe^{II}-O_2-Mb results in oxidation of NO• to nitrate and to the formation of Fe^{III}-Mb.[19] Under normoxic conditions, Fe^{II}-Mb can scavenge NO• and protect mitochondrial respiration from inhibition.[15] On the other hand, under hypoxic conditions, its nitrite reductase activity makes Fe^{II}-Mb a source of NO•, conferring protection

Received: April 4, 2016
Published: June 16, 2016

DOI: 10.1021/jacs.6b03456
J. Am. Chem. Soc. 2016, 138, 8476−8488

during ischemia/reperfusion injury.[16] The reaction of Fe^{II}-Mb with nitrite is slow with a bimolecular rate constant of 6 M^{-1} s^{-1} (20 °C, pH 7.0) and generates Fe^{III}-Mb,[20] which is reduced to Fe^{II}-Mb by metmyoglobin (MetMb) reductase.[21] In this study, we have examined a potential role for Mb in sulfide oxidation.

Sperm whale Fe^{III}-Mb is reported to bind sulfide with low affinity (18.5 μM at pH 7.5 and 20 °C)[22] similar to human Fe^{III}-Hb (K_D = 17 ± 2 μM at pH 7.4, 37 °C). In fact, the binding of sulfide to myoglobin has been exploited in the design of a fluorescence sensor to detect H_2S.[23] Covalent addition of sulfide to form sulfmyoglobin[9] is associated with the greening of meat.[24] However, the ability of myoglobin to catalyze sulfide oxidation has not been previously investigated. In this study, we report that, under aerobic conditions, Fe^{III}-Mb converts sulfide to thiosulfate and polysulfides and provide cryo-mass spectrometric and spectroscopic evidence for the formation of novel protein-bound oxidized sulfur species. Deficiency of persulfide dioxygenase (also known as ETHE1) in the mitochondrial sulfide oxidation pathway, leads to ethylmalonic encephalopathy.[25] This disorder presents with an unusual and severe depletion of cytochrome c oxidase in muscle and brain, whose molecular basis remains to be explained.[26] We speculate that impaired disposal of H_2S in ethylmalonic encephalopathy patients promotes its interaction with myoglobin, increasing muscle sulfide concentration and, consequently, leading to adverse effects on cytochrome c oxidase activity and stability.

EXPERIMENTAL SECTION

Materials. Equine skeletal muscle Fe^{III}-Mb, Na_2S nonahydrate, and L-cystine, H_2S solution (0.8 M) in tetrahydrofuran and xylenol orange were from Sigma (St. Louis, MO). Monobromobimane (FluoroPure grade) was from Molecular Probes (Grand Island, NY) and HEPES was from Fisher Scientific (Walham, MA). Recombinant human γ-cystathionase (CSE) was prepared as described previously.[27]

Sulfide Binding Studies. The concentration of Fe^{III}-Mb in 100 mM HEPES buffer, pH 7.4, was determined using an extinction coefficient of 188,000 M^{-1} cm^{-1} at 409 nm. For spectrophotometric analysis of Na_2S binding to Fe^{III}-Mb (10 μM in 100 mM HEPES buffer, pH 7.4), varying concentrations of Na_2S were added and the change in absorbance was monitored.

Reaction of Cysteine Persulfide (Cys-SSH) with Myoglobin. Fe^{III}-Mb (8 μM) in 100 mM HEPES buffer, pH 7.4 was incubated under aerobic conditions with 1 mM L-cystine and 1 μM human CSE at 37 °C. Under these conditions, Cys-SSH is formed.[28] Heme absorption spectra were recorded every 2 min over a 60 min period.

Stopped-Flow Spectroscopy. The kinetics of interaction between Fe^{III}-Mb and Na_2S was studied using an Applied Photophysics stopped-flow spectrophotometer (SX.MV18) inside an anaerobic chamber (Vacuum Atmospheres Co., Hawthorne, CA). To determine the dependence of the rate constant for formation of the iron-sulfide complex on the concentration of Na_2S, an anaerobic solution of Fe^{III}-Mb (5 μM before mixing in 100 mM HEPES buffer, pH 7.4) was mixed rapidly with various concentrations of Na_2S (0.02–2 mM before mixing) in the same buffer at 37 °C and the spectra were recorded. To determine the pH dependence of the rate constant for iron-sulfide complex formation, Fe^{III}-Mb (5 μM before mixing) was prepared in 100 mM buffer with pH ranging from 5.5 to 9.0 and rapidly mixed with 2 mM Na_2S (before mixing) in the same buffer. Borate, Tris and HEPES buffers were used for pH 9.0, 8.0, and 7.4, respectively. Citrate buffer was used for pH 6.0 and 5.5. The change in absorption at 409 nm was monitored at 25 °C. The data were fitted to a single exponential function.

Product Analysis. The products of Fe^{III}-Mb-dependent sulfide oxidation were characterized as follows. A mixture of Fe^{III}-Mb (100 μM) and Na_2S (1 mM) in 100 mM HEPES buffer, pH 7.4 was incubated aerobically or anaerobically at 25 °C. At the desired time points, samples were removed for analysis. Controls lacking Fe^{III}-Mb or Na_2S were set up in parallel.

Sulfane sulfur products were detected using cold cyanolysis as described previously.[10,29] The calibration curves for cold cyanolysis were linear between 0.01 and 1 mM sodium thiocyanate. For cold cyanolysis, 0.5 mL of the sample was mixed with 0.25 mL of a solution containing 62.5 mM potassium cyanide and 125 mM ammonium hydroxide. Samples were then incubated at 25 °C for 45 min. Then, Goldstein's reagent (0.75 mL) was added to each sample, the mixture was centrifuged at 13 000 × *g* for 3 min, and the absorbance of the supernatant was measured at 460 nm. Goldstein's reagent was made by dissolving 1.25 g of $Fe(NO_3)_3{\cdot}9H_2O$ in 12.5 mL of water and adding 13.1 mL of 70% HNO_3 (specific gravity 1.4) and water to a final volume of 50 mL.[29]

Sulfite, thiosulfate, and sulfide concentrations were determined by HPLC. Briefly, samples were derivatized with monobromobimane and analyzed using a Zorbax Eclipse XDB-C18 column (5 μm, 4.6 mm × 150 mm, Agilent), with a gradient of methanol as described previously.[10] The eluent was monitored using a fluorescence detector with the excitation wavelength set at 390 nm and emission at 490 nm. The column was calibrated with known concentrations of sulfite, thiosulfate, and sulfide.

H_2O_2 Analysis. The concentration of H_2O_2 was monitored using the xylenol orange assay.[30] For this, Na_2S (1 mM) was mixed with 100 μM Fe^{III}-Mb in 1 mL of 100 mM HEPES buffer, pH 7.4, and incubated at 25 °C in parallel with controls lacking Fe^{III}-Mb and Na_2S or Na_2S only. Aliquots (0.1 mL) were removed at the desired time points, injected into 1 mL of working reagent (1:100 v/v of reagents A/B where reagent A was 25 mM ferrous ammonium sulfate in 2.5 M H_2SO_4 and reagent B was 100 mM sorbitol and 125 μM xylenol orange in water), and incubated for 20 min at 25 °C, and the absorbance at 560 nm was recorded. A calibration curve was prepared using known concentrations of H_2O_2.

O_2 Consumption Assay. Oxygen consumption during the reaction of Fe^{III}-Mb with Na_2S was measured at 25 °C in a 1.5 mL Gilson-type chamber with a Clark-type oxygen electrode and magnetic stirrer as described previously.[10] A solution of 100 μM Fe^{III}-Mb in 100 mM HEPES buffer, pH 7.4, was placed in the chamber, and following stabilization of the background signal, Na_2S was added to a final concentration of 1 mM.

EPR Spectroscopy. For EPR analysis, Fe^{III}-Mb (200 μM final concentration) in 100 mM HEPES, pH 7.4 containing 20% glycerol was mixed with Na_2S (2 mM final concentration) and the sample was incubated aerobically at 25 °C. Aliquots (400 μL) were removed before the addition of Na_2S and at 5, 35, and 60 min after addition of Na_2S, and frozen in liquid N_2 in EPR tubes. EPR spectra were recorded at 14 K on a Bruker EMX spectrometer with a Bruker 4102-ST general purpose cavity and an Oxford liquid helium cryostat using the following settings: 5.00 G modulation amplitude, 100 kHz modulation frequency, 5000 G sweep width centered at 3000 G, 9.336 GHz microwave frequency, and 0.103 mW microwave power.

Resonance Raman Spectroscopy. The same samples were used for EPR and Raman spectroscopy. Similar samples were also made under anaerobic conditions. The resonance Raman measurements were performed using the 413.13 nm excitation line from a Kr^+ ion laser (Spectra Physics Beam Lok 2060-RS). Raman spectra were recorded at 77 K using an Acton two-stage TriVista 555 monochromator connected to a liquid nitrogen cooled CCD camera (Princeton instruments Spec-10:400B/LN). The samples were kept in an EPR coldfinger in liquid nitrogen at 77 K. The experiments were performed with a variable number of accumulations and exposure times to minimize the fluorescence background that generally increased with the sample reaction time. The total exposure time of the samples to the laser radiation was 10 min. Typical laser powers at the sample were in the 10–30 mW range. Relative wavenumbers (Raman shifts) were calibrated using sodium sulfate.

Mass Spectrometry. Fe^{III}-Mb (400 μM) was prepared in 20 mM ammonium carbonate buffer pH 7.4. For anaerobic measurements,

DOI: 10.1021/jacs.6b03456
J. Am. Chem. Soc. 2016, 138, 8476–8488

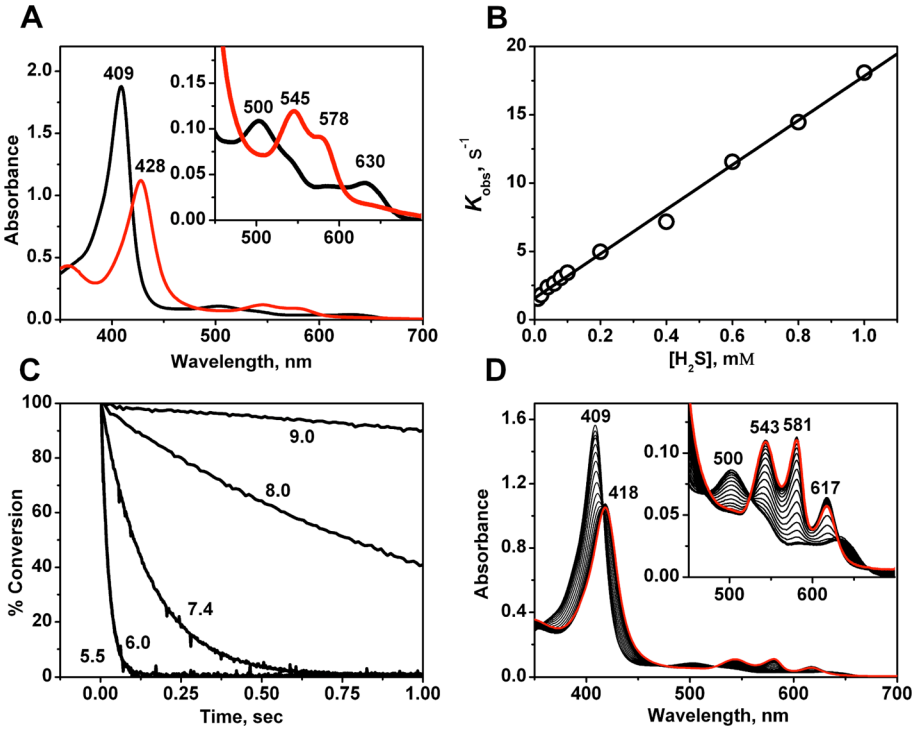

Figure 1. Spectral changes accompanying addition of sulfide or Cys-SSH to Fe^{III}-Mb. (A) Changes in the absorption spectrum of Fe^{III}-Mb (black, 10 μM in aerobic 100 mM HEPES buffer, pH 7.4 at 25 °C) 2 min after the addition of 1 mM Na_2S (red). The *inset* shows an expansion of the α/β region. (B) Dependence of k_{obs} for the formation of the ferric sulfide species on the concentration of total Na_2S. The k_{obs} values for the interaction of Fe^{III}-Mb with Na_2S were determined at 409 nm using stopped-flow absorption spectroscopy. In these experiments, anaerobic 5 μM Fe^{III}-Mb in 100 mM buffer, pH 7.4, 37 °C, was rapidly mixed with 0.02−2.0 mM Na_2S. Concentrations reported on the *x*-axis are after mixing. (C) The pH dependence of ferric−sulfide complex formation as determined using stopped-flow spectroscopy. Fe^{III}-Mb (5 μM) was prepared in buffers with different pH values as described in the "Experimental Section" and mixed at 25 °C under anaerobic conditions, with 2 mM Na_2S prepared in the same buffers. The pH values are indicated on the *curves*. The curves obtained at pH 5.5 and 6.0 overlap. (D) Electronic absorption changes of Fe^{III}-Mb induced by the addition of Cys-SSH. Fe^{III}-Mb (8 μM) in 100 mM HEPES buffer, pH 7.4 was mixed with human CSE (1 μM) and L-cystine (1 mM) under aerobic conditions at 37 °C. Spectra were recorded every 2 min, and the final spectrum at 60 min is shown in red. Under these conditions, Cys-SSH is formed in situ. The *inset* shows an expansion of the α/β region of the spectrum.

Fe^{III}-Mb was dissolved in degassed buffer in an argon-purged glovebox and kept in dark vials with polytetrafluoroethylene septa. A gastight syringe was used for handling the anaerobic samples. H_2S dissolved in THF (0.8 M) was diluted into 20 mM ammonium carbonate buffer in the glovebox. After mixing, the sample was incubated at room temperature for 30 min and before spraying, the sample was diluted 10-fold with 20 mM ammonium carbonate buffer pH 7.4 to a final concentration of 40 μM Fe^{III}-Mb and 400 μM H_2S.

Mass spectrometric (MS) measurements were performed on a UHR-ToF spectrometer maXis 4G (Bruker Daltonik, Bremen, Germany) coupled to a Bruker cryospray unit. The resolution of the ESI-ToF MS is at least 40.000 full-width at half-maximum. Detection was in the positive-ion mode. The flow rates were 300 μL/h. The drying gas (N_2), was held at 10 °C, and the spray gas (N_2) was held at 5 °C. The instrument was calibrated prior to each experiment via direct infusion of the Agilent ESI-ToF low concentration tuning mixture, which provided an m/z range of singly charged peaks up to 2700 Da in both ion modes.

X-ray Absorption Spectroscopy Analysis. Fe^{III}-Mb (2 mM in iron concentration) was prepared in 100 mM HEPES buffer, pH 7.4. Then, the solution was divided into three aliquots. The first aliquot was mixed with glycerol to a final concentration of 30% (v/v). To the second aliquot, H_2S in THF was added to a final concentration of 20 mM and the mixture was incubated aerobically for 60 min at 25 °C before addition of 30% glycerol (v/v). The third aliquot was incubated aerobically for 30 min at 37 °C with 4 mM cystine and 200 μM CSE. Then, glycerol was added to a final concentration of 30% (v/v). Immediately after mixing with glycerol, all samples were injected into Kapton wrapped lucite XAS sample cells, flash frozen, and stored in liquid N_2 until beam exposure.

XAS data were collected at the Stanford Synchrotron Radiation Lightsource on beamline 7−3 which is equipped with a Si(220) double-crystal monochromator with an upstream mirror for focusing and for harmonic rejection. Fluorescence spectra were collected using a 30-element Ge solid-state detector from Canberra. During data collection, the Oxford Instruments continuous-flow liquid helium cryostat was stabilized at 10 K. Iron K-edge electronic excitation data were collected using a 6 μm Mn filter placed between the cryostat and the detector to reduce unassociated scattering. An Fe foil spectrum was collected simultaneously with each protein spectrum for energy calibration. The first inflection point for the Fe foil was set to 7111.3 eV. Iron extended X-ray absorption fine structure (EXAFS) spectra were recorded using 5 eV steps in the pre-edge region (6900−7094 eV), 0.25 eV steps in the edge region (7095−7135 eV), and 0.05 $Å^{-1}$ increments in the EXAFS region (to k = 13.5 $Å^{-1}$), integrating from 1 to 20 s in a k^3-weighted manner. An average of 9 scans were collected for each sample to increase spectral signal-to-noise, and each scan took ~45 min to record. Samples were closely monitored for X-ray induced radiation damage and photoreduction. Each spectrum was measured using a 1 mm × 3 mm X-ray beam size so independent spectra could be collected at 9 individual positions in the sample, as X-ray induced photoreduction was observed as early as during the second scan on each independent sample position.

XAS spectra were processed and analyzed using the EXAFSPAK program suite written for Macintosh OSX.[31] Fluorescence scans corresponding to each detector channel were examined for spectral anomalies. Spectra were then averaged to enhance spectral signal-to-

DOI: 10.1021/jacs.6b03456
J. Am. Chem. Soc. 2016, 138, 8476−8488

noise ratios. A Gaussian function was used to fit background data within the spectral pre-edge region, and a three-region cubic spline was used for baseline subtraction within the EXAFS region. EXAFS data were converted to k space using an E_0 value of 7130 eV. Spectra were simulated using single and multiple scattering amplitude and phase functions generated using the Feff v8 software package integrated within EXAFSPAK. Single scattering models were calculated for oxygen, nitrogen, sulfur, and carbon coordination to simulate possible iron ligand environments. Calibrated scale factors (Sc) and model E_0 values were not allowed to vary during fitting; an Sc value of 0.95 was used for iron samples. Iron data were fit out to a k value of 14.0 $Å^{-1}$. Calibrations using Fe^{II} and Fe^{III} theoretical model compounds were used to determine the E_0 and Sc parameters. E_0 values for Fe-(O/N/C) and Fe−S interactions were set at −10.7 eV and −16.7 eV respectively, based on values obtained from fitting Fe model compounds.[32] EXAFS spectra were simulated using both filtered and unfiltered data; however, simulation results are presented only for fits to raw (unfiltered) data. Simulation protocols and criteria for determining the best fit were described previously.[33]

Theoretical Calculations. Density functional theory (DFT) calculations were employed to assess the feasibility of the nature of the sulfide adduct of Fe^{III}-Mb. All models consisted of a truncated porphyrin ligand and a methyl-imidazole to represent the coordinated histidine side chain. No outer-sphere residues were included in these models. All models were subjected to full geometry optimizations with ORCA version 3.02 or 3.03[34] using DFT. The polarized split valence (SV(P)) basis[35] and the SV/C auxiliary basis[35] were used for all atoms except Fe, its direct neighbors, and all non-hydrogen atoms of the exogenous ligand, for which Ahlrichs' valence triple-ξ with a polarization function basis set[36] was employed. Two functionals were used in these calculations for all models; namely, BP86[37,38] (pure functional) and B3LYP[39,40] (hybrid functional). Plots of the geometry-optimized models were generated using PyMOL.[41]

RESULTS

Binding of H_2S to Fe^{III}-Mb. A shift in the Soret band peak position from 409 to 428 nm was observed upon mixing Fe^{III}-Mb with an excess of Na_2S under aerobic conditions (Figure 1A). This shift was accompanied by a decrease in absorbance at 500 and 630 nm and an increase in absorbance at 545 and 578 nm with isosbestic points at 420, 482, 524, 613, and 660 nm. Identical spectral changes were observed when Fe^{III}-Mb was mixed with an excess of Na_2S under anaerobic conditions. Formation of low-spin six-coordinate ferric sulfide species has also been observed for H_2S binding to the model compound Met-hemoCD3, to neuroglobin and to the truncated hemoglobins Bs-trHb and Tf-trHb.[42−44] The kinetics of formation of the 428 nm Soret band, tentatively attributed to an Fe^{III}-$^{-}$SH-Mb species (Table 1), was determined under stopped flow conditions. From the dependence of k_{obs} on sulfide concentration (Figure 1B) a bimolecular rate constant of $(1.6 \pm 0.3) \times 10^4$ M^{-1} s^{-1} and a k_{off} value of 1.6 ± 0.2 s^{-1} were obtained, yielding a K_D of 96 ± 12 μM at pH 7.4 and 37 °C. A similar K_D value (84 ± 5 μM) was obtained by plotting the dependence of the change in absorbance of the 409 nm band on Na_2S concentration (not shown). It is important to note that these K_D values likely represent an upper limit since only ∼20% of the total sulfide exists as H_2S at pH 7.4. Adjusting for the concentration of dissolved H_2S at pH 7.4, the K_D values for sulfide binding to Fe^{III}-Mb are estimated to be 19 ± 2 μM and 17 ± 1 μM from the kinetic and thermodynamic data, respectively.

Table 1. Comparison of the UV−visible Absorption Properties of Myoglobin Derivatives

Myoglobin Species	Absorption maxima (nm)	Reference
Fe^{III}-Mb	409, 505, 630	66
Fe^{II}-Mb	434, 556	47, 66
Fe^{II}-O_2-Mb	416, 546, 580	66
Fe^{III}-$^{-}$SH-Mb	428, 545, 578	9, this study
Fe^{IV}-Mb	421, 548, 582	66
Fe^{III}-sulf-Mb	408, 595, 715	9
Fe^{II}-sulf-Mb	424, 617	66
Fe^{II}-O_2-sulf-Mb	408, 623	66

The rate constant for the formation of the 428 nm species was found to be inversely proportional to pH (Figure 1C) consistent with the initial binding of H_2S to Fe^{III}-Mb or to the protonation of a group on Fe^{III}-Mb favoring sulfide binding.

Interaction of Cysteine Persulfide (Cys-SSH) with Fe^{III}-Mb. In addition to producing H_2S, the transsulfuration enzyme, CSE, synthesizes Cys-SSH (eq 1) from cystine, the oxidized

$$\text{Cys-SS-Cys} \rightarrow \text{Cys-SSH} + \text{Pyruvate} + \text{NH}_3 \quad (1)$$

form of cysteine.[28,45] We examined the effect of Cys-SSH generated *in situ* on the absorption spectrum of Fe^{III}-Mb (Figure 1D). A shift in the Soret peak from 409 to 418 nm and the appearance of 543 and 581 nm absorption bands were observed, which are similar to but distinct from oxy-Fe^{II}-Mb (Table 1). While the identity of the product with the 418 nm Soret peak is not known, it could represent an Fe^{II}−SSH type of species. In addition, a peak at 617 nm was observed that is typical of Fe^{II}-sulfmyoglobin (Table 1) in which sulfide is covalently bound to the porphyrin ring.[9]

H_2S Oxidation Products. In the presence of 100 μM Fe^{III}-Mb, ∼1 mM sulfide was consumed in <120 min (Figure 2A). During the same time, ∼20% of the sulfide was lost from the control sample lacking Fe^{III}-Mb. Product analysis revealed accumulation of ∼160 μM thiosulfate (Figure 2B), accounting for 320 μM (∼40%) sulfur consumed in reactions catalyzed by myoglobin. An almost equivalent concentration of sulfur was retrieved as sulfane sulfur by cold cyanolysis of the reaction mixture (Figure 2C). The sulfane sulfur pool was protein bound since cold cyanolysis did not detect any product in the filtrate obtained using a Centricon concentrator. Cold cyanolysis is expected to release up to the penultimate sulfur in a hydropolysulfide chain attached to iron, leaving up to ∼12.5% of the original sulfur on myoglobin. We note that if oxygenation occurs at sulfur atoms in the catenated sulfur species bound to iron, they will not be detected by cold cyanolysis, leading to an underestimation of the sulfur tied up in the hydropolysulfide chains. As discussed below, MS analysis provides evidence for the presence of such species in the reaction mixture.

Under anaerobic conditions, sulfide consumption was approximately stoichiometric with Fe^{III}-Mb concentration (∼100 μM) instead of catalytic (∼800 μM) as observed under aerobic conditions (Figure 2D). This is consistent with O_2 being needed for the further conversion of initially bound sulfide to products.

Kinetics of O_2 Consumption and H_2O_2 Formation. The formation of reactive oxygen species (superoxide anion and H_2O_2) has been proposed during Fe^{III}-Hb-catalyzed oxidation of sulfide[10] and, by analogy, for Fe^{III}-Mb. The xyenol orange assay was used to detect H_2O_2 and to compare the kinetics of its formation to that of O_2 consumption monitored using an oxygen electrode (Figure 3). The rate of O_2 consumption (Figure 3A) was similar to that of sulfane sulfur and thiosulfate

DOI: 10.1021/jacs.6b03456
J. Am. Chem. Soc. 2016, 138, 8476−8488

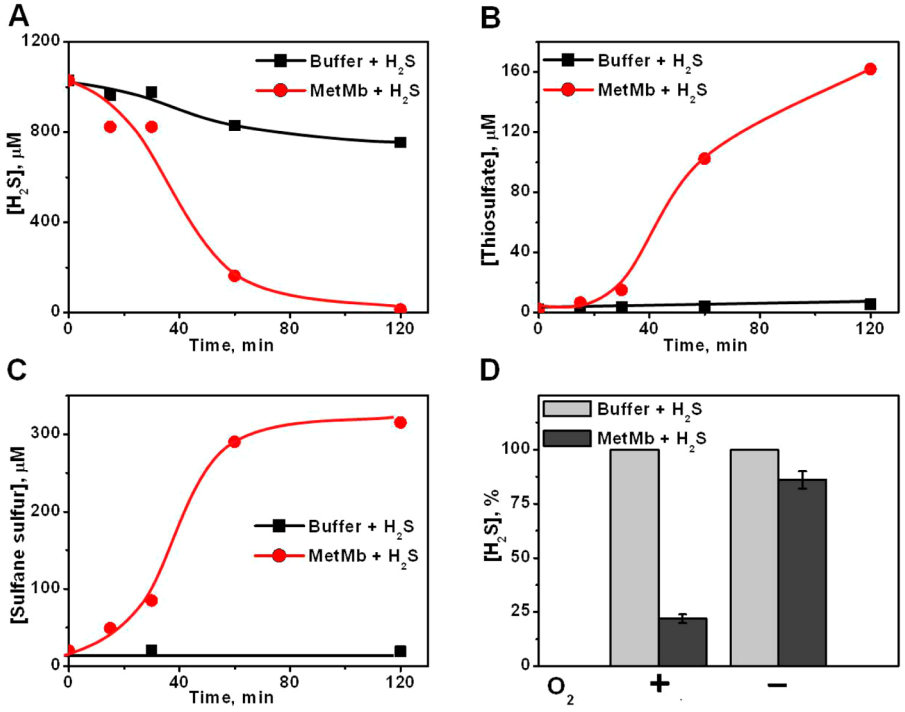

Figure 2. Kinetics of H_2S disappearance (A) and thiosulfate (B) and sulfane sulfur (C) formation in the presence of Fe^{III}-Mb. Na_2S (1 mM) was added to Fe^{III}-Mb (100 μM) in 100 mM HEPES buffer, pH 7.4, at 25 °C under aerobic conditions. (D) Concentration of H_2S remaining after 1 h following addition of Na_2S (1 mM) to 100 μM Fe^{III}-Mb in 100 mM HEPES buffer, pH 7.4, at 25 °C under aerobic and anaerobic conditions. The concentration of H_2S in the sample lacking Fe^{III}-Mb (gray) is represented as 100%.

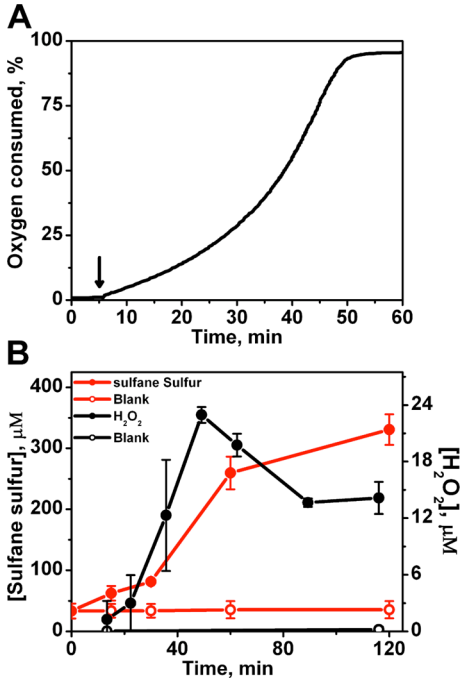

Figure 3. Kinetics of O_2 consumption (A) and sulfane sulfur and H_2O_2 formation (B) in a solution containing 100 μM Fe^{III}-Mb in 100 mM HEPES buffer, pH 7.4, at 25 °C after addition of 1 mM Na_2S. *A*. Representative graph of O_2 consumption by Fe^{III}-Mb following addition of Na_2S (indicated by arrow). In part B, the data represent the mean ± SD of three experiments. H_2O_2 and sulfane sulfur concentrations were determined as described in the Experimental Section.

formation (Figure 2B,C). A lag phase extending for ~30 min was followed by a rapid phase in which O_2 consumption and thiosulfate and sulfane sulfur formation were observed. A possible explanation of the lag phase is provided in the Discussion section. A rise in H_2O_2 preceded formation of the sulfane sulfur products (Figure 3B). The maximal accumulation of H_2O_2 represented ~6% that of the sulfane sulfur concentration.

EPR Spectroscopic Characterization of Sulfide Oxidation by Fe^{III}-Mb. Ferric myoglobin exhibits a characteristic high spin EPR spectrum with g = 5.92 (Figure 4). Addition of an excess of sulfide under aerobic conditions results in the appearance of a rhombic low-spin signal with g values of 2.57, 2.27, and 1.85, respectively. Double integration of the low-spin

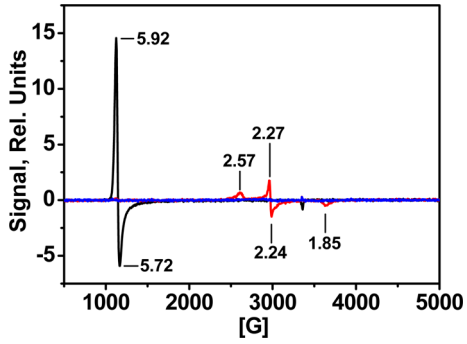

Figure 4. EPR spectroscopic characterization of Fe^{III}-Mb following the addition of Na_2S. The spectra show Fe^{III}-Mb (200 μM, black) in 100 mM HEPES buffer, pH 7.4 containing 20% glycerol (v/v) and after 5 min (red) or 35 min (blue) incubation with Na_2S (2 mM) at 25 °C, under aerobic conditions. The EPR settings are described in the Experimental Section.

DOI: 10.1021/jacs.6b03456
J. Am. Chem. Soc. 2016, 138, 8476−8488

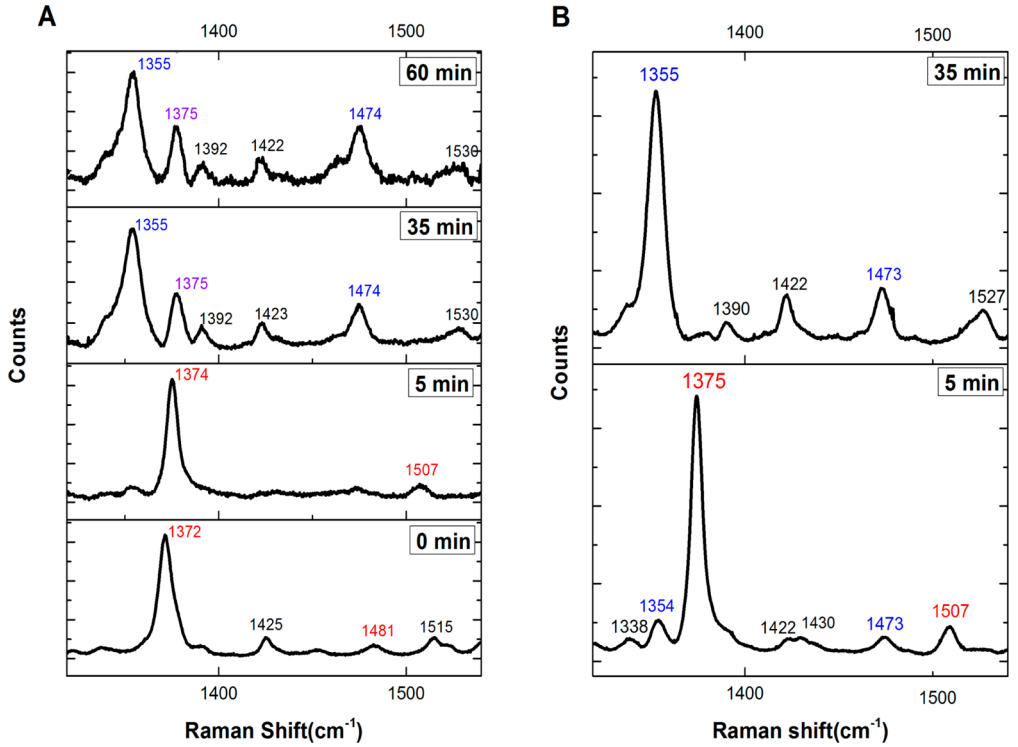

Figure 5. Time-dependent changes in the resonance Raman spectrum of Fe^{III}-Mb following exposure to sulfide under aerobic (A) and anaerobic (B) conditions. The high-energy region of the spectrum is shown for the reaction of Fe^{III}-Mb (200 μM) with sulfide (2 mM) in 100 mM HEPES buffer, pH 7.4 containing 20% glycerol (v/v). The excitation wavelength was 413.1 nm, and the laser power was 10 mW at the sample. The spectrum of each sample was collected over a period of ~10 min and represents the average of six accumulations with 100 s exposure time. The bands corresponding to high-spin Fe^{III}-Mb (0 min, ν_4 = 1372 cm^{-1} and ν_3 = 1481 cm^{-1}) and low-spin Fe^{III}-$^{-}$HS Mb (5 min, ν_4 = 1374 cm^{-1} and ν_3 = 1507 cm^{-1}) are shown in red. The ν_4 (1355 cm^{-1}) and ν_3 (1474 cm^{-1}) bands corresponding to ferrous-Mb with an unknown ligand (at 35 and 60 min) are shown in blue, and the ν_4 band corresponding to oxy-Fe^{II}-Mb (1375 cm^{-1}) is shown in purple.

signal indicated that it corresponds to up to 65% of the total iron concentration in the sample. The EPR spectrum is virtually identical to that reported previously for ferric myoglobin with a sulfide ligand.[46,47] An EPR signal was not observed at 35 and 60 min after addition of sulfide.

Resonance Raman Spectroscopic Characterization of Sulfide Oxidation by Fe^{III}-Mb. The resonance Raman spectra of Fe^{III}-Mb at 0 (i.e., without Na_2S), 5, 35, and 60 min after addition of Na_2S are shown in Figure 5. The well-known oxidation and spin state marker bands of heme can be used to analyze changes in the heme during the reaction of Mb with Na_2S.[48,49] At t = 0, the 1372 (ν_4) and 1481 cm^{-1} (ν_3) bands, characteristic of high-spin Fe^{III}, are observed (Figure 5A). After 5 min, the ν_4 band (corresponding to the Fe^{III} oxidation state) is unchanged while the ν_3 band is shifted to 1507 cm^{-1} in aerobic (Figure 5A) and anaerobic (Figure 5B) samples, consistent with sulfide binding and forming a six-coordinate low-spin Fe^{III}-$^{-}$SH species. Similar resonance Raman spectra have been reported for the formation of low-spin six-coordinate ferric sulfide adducts in the truncated hemoglobins Bs-trHb and Tf-trHb.[42] Initial formation of a six-coordinate low-spin Fe^{III}-sulfide species is also consistent with our EPR spectroscopy results (Figure 4).

At 35 min, a time at which O_2 consumption and product formation are underway (Figures 2,3), high spin Fe^{II}-Mb is the major species, indicated by the shift in the oxidation state marker band to 1355 cm^{-1} and the spin state marker to 1474 cm^{-1}. It is unclear whether the 1355 cm^{-1} corresponds to single or multiple high spin ferrous intermediates that accumulate during catalytic sulfide oxidation. In addition, a signal at 1375 cm^{-1} appears in the aerobically prepared sample (Figure 5A) that is assigned to oxy myoglobin, Fe^{II}-O_2-Mb.[48,49] It is absent in the anaerobically prepared sample (Figure 5B). The Fe^{II}-O_2-Mb adduct is unique with respect to showing the oxidation state marker band in the ferric energy range, yet being diamagnetic (and hence EPR silent). The assignment of the Fe^{II}-O_2 adduct is further supported by the appearance of a new Raman feature at ~570 cm^{-1} in the spectrum of the aerobic (Figure 6A) but not the anaerobic (Figure 6B) sample, which has previously been assigned as the Fe^{II}-O_2 stretch.[48,49] Unfortunately, as the reaction progresses, the fluorescence background in the Raman spectra increases, reducing spectral quality. The ratio of the 1355:1375 cm^{-1} band intensities remains steady between 35 and 60 min during which time sulfide is maximally consumed and its oxidation products are formed (Figure 2A–C). The band at 1355 cm^{-1} is a ferrous Mb species, potentially with a sulfur ligand. Interestingly, this species has a ν_3 band at 1474 cm^{-1}, indicating a high-spin ferrous center. The fact that the complex is high-spin suggests the presence of a weak sixth ligand. Additional spectroscopic studies are in progress for assigning this species.

The low frequency region of the resonance Raman spectrum shows several differences between 0 and 35 min (Figure 6). In addition to the 570 cm^{-1} band seen in the aerobic sample, other low-energy features are observed at 365, 502, 533, and 545 cm^{-1} in the spectrum recorded at 35 min (Figure 6A). The 500 cm^{-1} band, but not the others, is also seen in the anaerobically prepared sample (Figure 6B). The identity of the

DOI: 10.1021/jacs.6b03456
J. Am. Chem. Soc. 2016, 138, 8476–8488

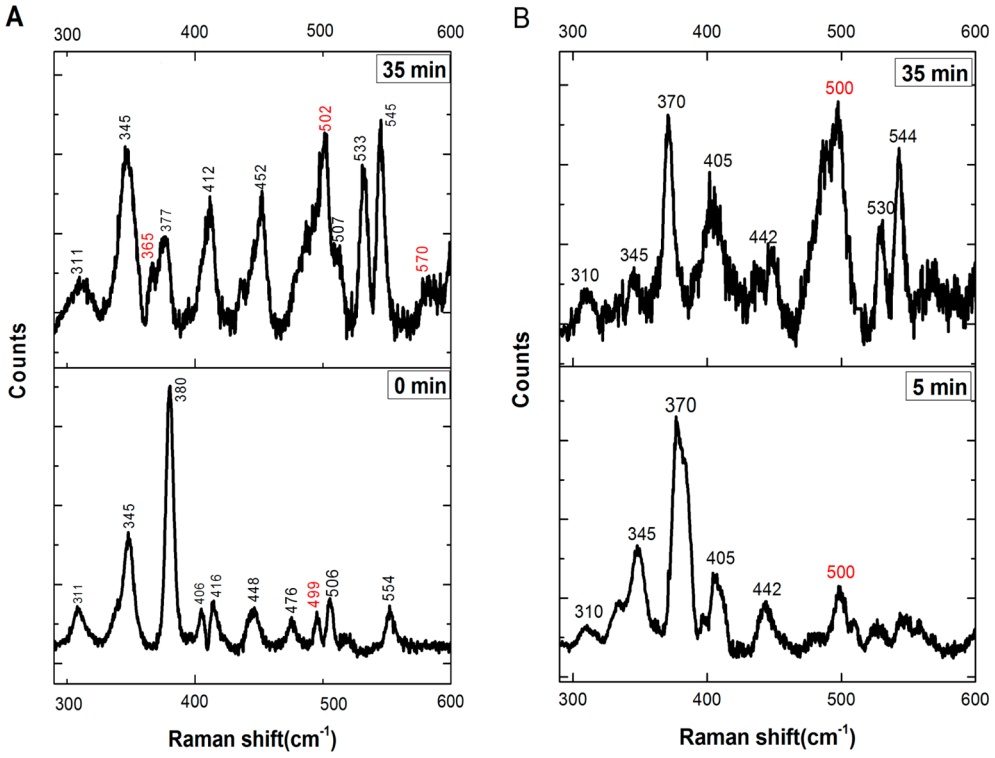

Figure 6. Lower energy region of the resonance Raman spectrum for Fe^{III}-Mb treated with sulfide under aerobic (A) and anaerobic (B) conditions. The samples were the same as those in Figure 5. The spectra represent the average of three accumulations with 180 s exposure time. The formation of Fe^{II}-O_2-Mb after 35 min is indicated by the appearance of the band at 570 cm^{-1}. A subset of bands in the low frequency region of the spectra that are discussed in the text are labeled in red.

species responsible for the bands in the low frequency is not known. A band at 365 cm^{-1} was tentatively assigned as the Fe−S stretching mode of the low spin Fe^{III}−sulfide complex of microperoxidase formed under anaerobic conditions[50] and hemoglobin I from *Lucina pectinata*.[51] The 365 cm^{-1} band in sulfide-treated myoglobin is observed only under aerobic conditions (compare Figures 6A and B) and is insensitive to the presence of deuterated buffer (not shown). Deuterium labeling of a ferric sulfide species would give Fe^{III}−SD_2 (or Fe^{III}−^{-}SD) and should induce a small shift in the Fe−S stretching frequency to lower energy. Since this is not observed experimentally, we conclude that the 365 cm^{-1} band in myoglobin does not represent the Fe−S stretching mode of an Fe^{III}−SH_2) adduct. The presence of a ferrous hydrodisulfide intermediate is, however, not ruled out by the isotope data.

XANES and EXAFS Analyses of Sulfide- and Cys-SSH-Treated Fe^{III}-Mb. The XANES spectra of Fe^{III}-Mb, Fe^{III}-Mb + Na_2S, and Fe^{III}-Mb + Cys-SSH were compared to those of the model compounds $FeSO_4$ and $Fe_2(SO_4)_3$ (Figure 7). The first inflection point edge energies, which correlate with the average iron oxidation state of iron in each sample, were 7124.4 eV (Fe^{III}-Mb), 7125.2 eV (Fe^{III}-Mb + Na_2S), and 7125.0 eV (Fe^{III}-Mb + Cys-SSH), respectively. For reference, the edge energies for the standards were 7122.9 eV (Fe^{II}) and 7126.3 eV (Fe^{III}), indicating that the XAS samples were a mixture of ferrous and ferric iron. The preedge 1s → 3d regions in the Mb XANES spectra are consistent with iron existing in a mixture of high-spin Fe^{II} and Fe^{III} states. The preedge transition energies and peak integrated areas were as follows: 7112.2 eV and 3.28 (±1.93) × 10^{-2} eV^2 (Fe^{III}-Mb), 7112.5 eV and 9.01 (±0.95) × 10^{-2} eV^2 (Fe^{III}-Mb + Na_2S), and 7112.5 eV and 11.65 (±1.95) × 10^{-2} eV^2 (Fe^{III}-Mb + Cys-SSH), consistent with values

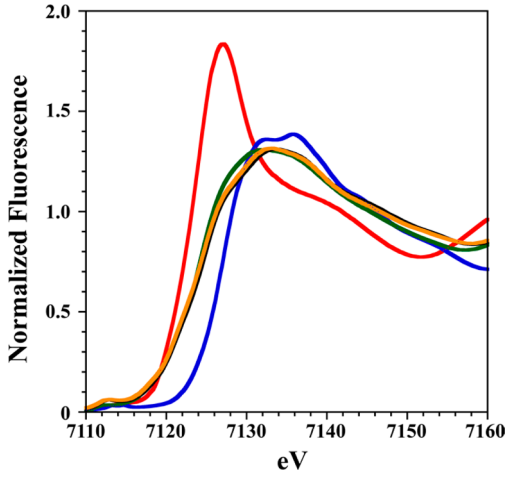

Figure 7. Normalized Fe X-ray absorption near edge structure (XANES) spectra of Fe^{III}-Mb (green), Fe^{III}-Mb + Na_2S (black), and Fe^{III}-Mb + Cys-SSH (orange). XANES spectra of samples are compared to standards, $Fe^{II}SO_4$ (red) and $Fe^{III}SO_4$ (blue) to determine average iron oxidation state. First inflection point edge energies are 7124.4 eV (Fe^{III}-Mb), 7125.2 eV (Fe^{III}-Mb + Na_2S), and 7125.0 eV (Fe^{III}-Mb + Cys-SSH), respectively. In comparison, the edge energies for the standards are 7122.9 eV ($Fe^{II}SO_4$) and 7126.3 eV ($Fe^{III}SO_4$).

reported for high spin Fe^{II} and Fe^{III} that are either five- or six-coordinate as well as with published XAS data on related globins.[52,53] The experiment was tightly controlled for photoreduction, a common occurrence with redox active metals exposed to high intensity radiation.[54]

DOI: 10.1021/jacs.6b03456
J. Am. Chem. Soc. 2016, 138, 8476−8488

The EXAFS data and Fourier transform for each sample are shown in Figure 8. The Fe^{III}-Mb data are best fit with five N-donor ligands with an Fe−N bond length of 2.03 Å (Table 2). In addition, there are four individual Fe−C vectors with lengths of 3.06, 3.41, 4.09, and 4.48 Å, which can be attributed to single and multiple scattering signals from the porphyrin ring. The data obtained for the sulfide-treated Fe^{III}-Mb sample are best fit in the Fe nearest neighbor environment with 3.5 Fe−N bonds at 2.02 Å and 0.5 Fe−S bonds at 2.16 Å. The Fe−S bond length is shorter than the 2.25 Å predicted from the Cambridge structural database for an FeN_5S_1 species but similar to the 2.18−2.19 Å Fe−S bond lengths reported for an Fe^{III}-cytochrome P450[55] and for Fe^{II}-*meso*-tetra(*α*,*α*,*α*,*α*-*o*-pivalamidophenyl)-porphyrin-2-methylimidazole.[56] The low occupancy of the sulfur site indicates a mixture of species as also noted for the XANES data. Only ∼65% of the Fe^{III}-Mb was converted to the sulfur ligated species based on the UV−visible absorption spectrum of the sample (not shown). The mixture resulted from the high sample concentration needed for XAS studies (2 mM heme iron) and the inability to provide a 100-fold excess of H_2S needed to fully convert Fe^{III}-Mb to the sulfide-bound form. The incomplete conversion of the starting ferric species explains the partial occupancy of the distal sulfur ligand. There are four individual Fe−C vectors with lengths of 3.06, 3.41, 4.08, and 4.47 Å, which match single and multiple scattering signals from the porphyrin ring (Table 2).

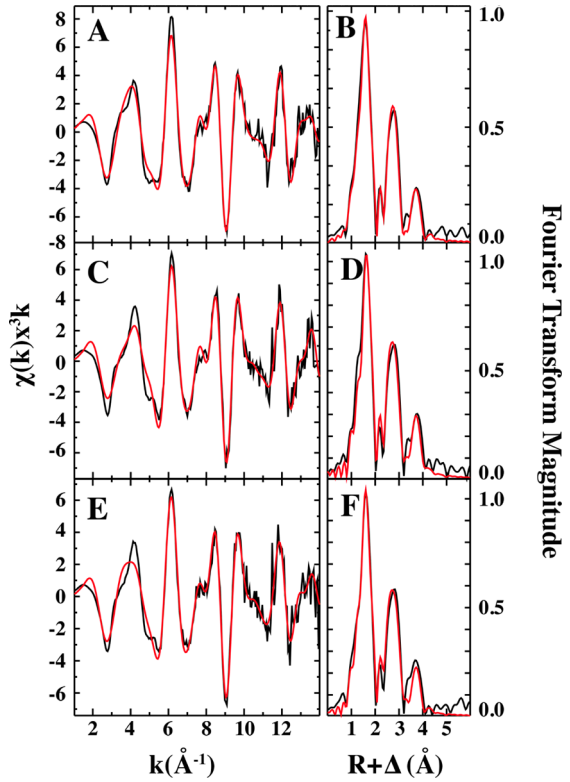

Figure 8. Comparison of Fe EXAFS and Fourier transforms of the EXAFS for empirical (black) and theoretical (red) spectra. Raw k^3-weighted EXAFS and Fourier transform of the EXAFS for Fe^{III}-Mb in panels A and B, respectively. EXAFS and Fourier transforms for Fe^{III}-Mb + Na_2S shown in panels C and D, respectively. EXAFS and Fourier transforms for Fe^{III}-Mb + Cys-SSH shown in panels E and F, respectively.

The EXAFS data of the Cys-SSH-treated sample are best fit in the Fe nearest neighbor environment with 3.5 Fe−N bonds at 2.02 Å and 0.25 Fe−S bonds at 2.19 Å. This sulfur content is even lower than that in the sulfide-treated sample, but the Fe−S bond length is slightly longer. Detection of an Fe−S bond is surprising since *a priori*, Cys-SSH is not expected to coordinate via a sulfur atom to the iron. However, Cys-SSH is unstable and can react with a second molecule of Cys-SSH to release H_2S forming Cys-SSS-Cys.[28] The low occupancy of the distal sulfur ligand can be attributed to the high concentration of Fe^{III}-Mb used relative to that of Cys-SSH, which was generated *in situ* by the enzymatic activity of CSE as described in the Experimental Section. In addition to the Fe−S vector, there are four individual Fe−C vectors with lengths of 3.07, 3.40, 4.09, and 4.49 Å, consistent with single and multiple scattering signals from the porphyrin ring (Table 2).

Table 2. Summary of Fe EXAFS Simulations[g]

Nearest-Neighbor Ligand Environment[a]					Long Range Ligand Environment[a]				
Sample	Atom[b]	*R* (Å)[c]	C.N.[d]	σ^{2e}	Atom[b]	*R* (Å)[c]	C.N.[d]	σ^{2e}	F'^f
Mb	N	2.03	5	4.38	C	3.06	5	1.44	0.43
					C	3.41	4	4.64	
					C	4.09	3	3.69	
					C	4.48	5	1.79	
Mb + Na_2S	N	2.02	3.5	3.78	C	3.06	5	2.36	0.46
	S	2.16	0.5	5.89	C	3.41	3	1.88	
					C	4.08	3	2.48	
					C	4.47	5	1.37	
Mb + Cys-SSH	N	2.02	3.5	3.43	C	3.07	6	4.09	0.49
	S	2.19	0.25	5.71	C	3.40	3	1.71	
					C	4.09	3	2.83	
					C	4.49	4	2.19	

[a]Each row represents an independent metal−ligand scattering environment. [b]Scattering atoms: N (nitrogen), S (sulfur), C (carbon). [c]Average metal−ligand bond length. [d]Average metal−ligand coordination number. [e]Average Debye−Waller factor (Å × 10^3). [f]Number of degrees of freedom weighted mean square deviation between experimental and theoretical data. [g]The XANES data are consistent with the samples being an approximately 50:50 mix of the ferric and ferrous states.

DOI: 10.1021/jacs.6b03456
J. Am. Chem. Soc. 2016, 138, 8476−8488

MS Analysis of the Reaction of Sulfide with Fe^{III}-Mb. The chemical identities of the species formed during aerobic incubation of Fe^{III}-Mb with H_2S were probed with ultrahigh-resolution ESI ToF cryo-MS, which allowed measurements to be made at 5 °C. The mild and low-temperature ionization conditions prevent decomposition of coordination complexes and were critical to the observation of oxidized sulfur species. The signals from the Fe^{III}-Mb sample nicely matched the predicted isotopic distribution (Figure 9, lower spectrum).

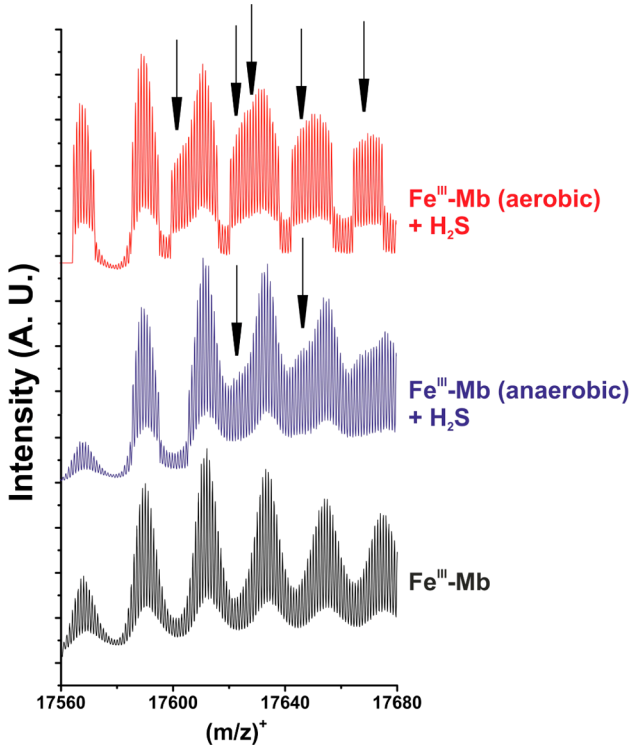

Figure 9. Deconvoluted mass spectra of Fe^{III}-Mb (black), Fe^{III}-Mb treated anerobically with a 10-fold excess of H_2S (blue) and Fe^{III}-Mb treated aerobically with a 10-fold excess of H_2S (red). The arrows indicate the appearance of major new species that are not seen in the spectrum of Fe^{III}-Mb alone. In the middle spectrum, a shoulder is seen on the peak with the highest m/z value. It corresponds to $[Mb(Fe\text{-}SH_2) - H + 2Na]^+$. All species are presented as singly charged.

Addition of a 10-fold excess of H_2S under anaerobic conditions led to minor spectral changes, with the appearance of two new peaks (Figure 9 middle spectrum). Based on the isotopic distribution, those peaks were assigned as $[Mb(Fe\text{-}SH_2) + H]^+$ and $[Mb(Fe\text{-}SH_2) + Na]^+$, both of which correspond to the coordination of one molecule of H_2S to myoglobin with zero and one sodium ion, respectively. Addition of a 10-fold excess of H_2S under aerobic conditions gave a much more complex mixture of species (Figure 9, top spectrum), indicating that different products are formed when O_2 is present. Besides the above-mentioned H_2S coordinated species, we observed coordination of H_2S_2 ($[Mb(Fe{-}S_2H_2)]$), HSO_3^- ($[Mb(Fe\text{-}(SO_3H)^-]$), and $S_2O_2H_2$ ($[Mb(Fe\text{-}(S_2O_2H_2)]$) (Figure 10). While we cannot rule out that the sulfur species are simply protein bound (i.e., in the active site), we assign them as iron bound species for the following reasons: (i) the Soret band of sulfide-treated myoglobin indicates formation of iron-bound species as the reaction progresses, and (ii) hydropolysulfides formed during catalytic sulfide oxidation are not observed in solution contrary to what would be expected if they were released from the iron. As discussed below, several of these species correspond to intermediates that we proposed previously to be formed in the reaction of Fe^{III}–Hb with H_2S.[10]

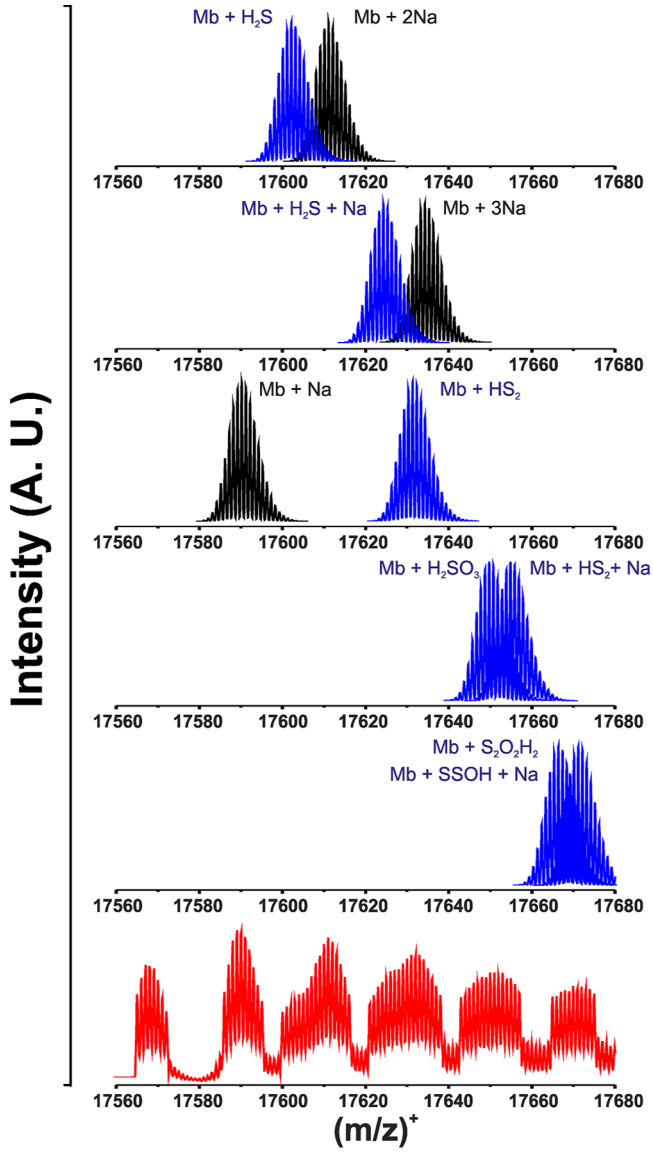

Figure 10. Speciation of the peaks observed in MS of Fe^{III}-Mb treated with an excess of H_2S (red spectrum). For clarity the simulated isotopic distribution of species seen in the spectrum of Fe^{III}-Mb alone is presented as black, while the new peaks that represent putative intermediates are presented in blue. All species are presented as single-charged.

DISCUSSION

The reaction between sulfide and ferryl hemeproteins to generate the corresponding covalently modified sulfheme species has been studied extensively.[57] In contrast, the ability of hemeproteins to support catalytic sulfide oxidation had not been appreciated until recently when we demonstrated that Fe^{III}–Hb converts sulfide to thiosulfate and iron-bound hydropolysulfides.[10] While binding of sulfide to Fe^{III}-Mb has been described earlier,[46,47] its capacity to support oxidative reactions has not been previously reported. Binding of sulfide to Fe^{III}-Mb results in a red shift of the Soret peak from 409 to

DOI: 10.1021/jacs.6b03456
J. Am. Chem. Soc. 2016, 138, 8476–8488

428 nm and in the appearance of β/α bands at 545 and 578 nm, respectively (Figure 1, Table 1). The bimolecular rate constant for binding of sulfide to Fe^{III}-Mb ($(1.6 \pm 0.3) \times 10^4$ M^{-1} s^{-1}) is 5-fold higher than that for Fe^{III}–Hb (3.2×10^3 M^{-1} s^{-1}) at pH 7.4 and 37 °C.[10] The k_{off} value is also higher for Mb (1.5 ± 0.2 s^{-1}) than for Hb (0.053 ± 0.008 s^{-1}), leading to an ~5.5-fold larger K_D for Fe^{III}-Mb (94 ± 12 μM) versus Fe^{III}–Hb (17 ± 2 μM). The sulfide affinities of hemoglobins specialized for H_2S delivery in organisms that subsist in sulfide-rich environments are quite a bit higher. For example, Hb1 from *L. pectinata* exhibits a K_D for sulfide of 3.4 nM and heme reduction is proposed as a prerequisite for sulfide release and delivery to symbiotic bacteria.[22]

The kinetics of sulfide interaction with microperoxidase, a hemeprotein model lacking stabilizing distal heme interactions, are interesting to compare to those of Fe^{III}-Mb. Microperoxidase, which also forms a low-spin ferric sulfide species, exhibits similar association (2.6×10^4 M^{-1} s^{-1} at pH 6.8, 25 °C) and dissociation ($k_{off} = 5.7 \pm 0.1$ s^{-1}) rate constants yielding a K_D value of ~220 μM.[50] Binding of sulfide to microperoxidase was only monitored under anaerobic conditions, and iron reduction was not observed.

Based on multiple spectroscopic analyses, we assign the initial sulfide adduct formed after deprotonation, as an Fe^{III}-$^-$SH species (Figure 11, [**1**]). This assignment is consistent with the disappearance of the high-spin Fe^{III}-Mb EPR signal and the appearance of a new signal associated with a low-spin, six-coordinate species (Figure 4) that is very similar to the spectra reported previously for Fe^{III}-Mb sulfide[46,47] and Fe^{III}-Hb sulfide.[10] The capture of an $[Mb(Fe\text{-}SH_2) + H]^+$ intermediate by cryo-MS (Figures 9, 10) also supports formation of an iron-sulfide species. The resonance Raman spectrum obtained 5 min after the addition of sulfide in the absence or presence of O_2 is consistent with the presence of a low-spin six-coordinate ferric species (Figure 5). The Fe–S stretching mode is often mixed with other vibrations and not necessarily resonance-enhanced upon laser excitation into the Soret band (e.g., in high-spin ferric cytochrome P450cam),[58,59] making its detection difficult. Together with the prohibitive expense of ^{34}S-labeling experiments, positive identification of this mode is challenging. In cystathionine β-synthase, which contains a low spin six-coordinate heme with a cysteine ligand, the ν(Fe–S) mode was detected at 312 cm^{-1} and confirmed by a 3 cm^{-1} shift upon global ^{34}S-labeling.[60] The frequency predicted by DFT calculations for the ν(Fe–S) mode in low-spin Fe^{III}-$^-$SH [**1**] is 328 cm^{-1} (vide infra). In the resonance Raman spectrum obtained 5 min after exposure of myoglobin to Na_2S (Figure 6), an obvious candidate for the ν(Fe–S) mode is not seen.

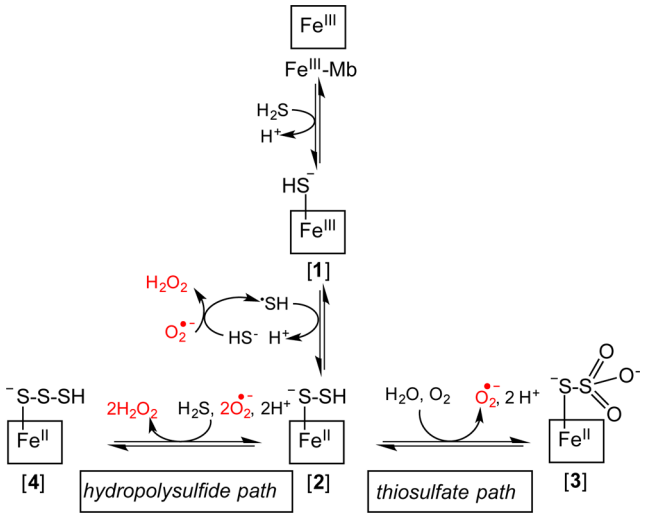

Figure 11. A minimal reaction mechanism postulated for sulfide oxidation by Fe^{III}-Mb. This figure is adapted from the mechanism originally postulated for ferric hemoglobin,[10] and the reactive oxygen species that are produced as side products, are shown in red. The stoichiometry of oxygen consumed to sulfide oxidized is presently not known and the mechanistic details between [**2**] and either [**3**] or [**4**] have been omitted for simplicity.

Under anaerobic conditions, the stoichiometry of H_2S consumed roughly equals that of the heme iron present, consistent with a simple binding event (Figure 2D). Sulfide binding to heme under anaerobic conditions is supported by the cryo-MS data, which reveal the presence of only a monosulfide adduct (Figure 9, middle spectrum). In contrast, under aerobic conditions, a significant excess of H_2S is consumed in the presence of Fe^{III}-Mb, indicating O_2-dependent catalytic turnover of sulfide (Figure 2A,D) as observed previously with Fe^{III}-Hb.[10] However, unlike the situation with hemoglobin in which O_2 consumption is observed immediately upon addition of excess sulfide, a noticeable lag phase is observed with myoglobin, which is paralleled by the rate of appearance of products (Figure 2A–C). While the origin of the lag phase is presently unclear, one possibility is that it could be due to the requirement for O_2-dependent generation of $HS^{\bullet}$, needed for the conversion of [**1**] to [**2**] (Figure 11). The apparently lower reactivity of the sulfide adduct of myoglobin toward O_2 and the higher on and off rates might favor its function as a storehouse for sulfide.

The conversions of the sulfide ligand in Fe^{III}-$^-$SH-Mb to thiosulfate and iron-bound polysulfides represent chemically challenging transformations. The postulated minimal mechanism (Figure 11) does not readily lend itself to experimental evaluation since the various intermediates are indistinguishable by most spectroscopic methods. We have therefore used a combination of cryo-MS to directly trap intermediates depicted in the model (Figure 11) and DFT calculations to evaluate the feasibility of the postulated intermediate [**1**]. Spin-unrestricted DFT geometry optimizations for a model of [**1**] containing an H_2S axial ligand converged to a low spin Fe^{III}–SH_2 complex with negligible spin density on the sulfur atom irrespective of the functional used. This assignment is consistent with the EPR (Figure 4) and resonance Raman (Figure 5) data, which show formation of a low-spin ferric species 5 min after sulfide addition. An alternative model of [**1**] featuring an $^-$SH ligand was also evaluated computationally (Figure 12, [**1**]; note that only the results obtained with the B3LYP functional are shown). By imposing an $S = {}^1/_2$ ground state as required by our EPR data, the DFT geometry optimizations using both functionals converged to low-spin Fe^{III}-$^-$SH complexes with modest to small spin density on the S atom. As expected, the Fe–S bond lengths for the singly deprotonated species is considerably shorter (2.24 Å) than in the doubly protonated counterparts (~2.5 Å). Computations were also performed for the $S = {}^3/_2$ and $^5/_2$ states using the BP86 functional. While the $S = {}^3/_2$ calculation did not converge, the one for the $S = {}^5/_2$ state did. The electronic structure of the $S = {}^5/_2$ model can be described as a resonance hybrid of high-spin Fe^{III}-$^-$SH and high-spin Fe(II)-$^{\bullet}$SH limiting descriptions. However, the S =

DOI: 10.1021/jacs.6b03456
J. Am. Chem. Soc. 2016, 138, 8476–8488

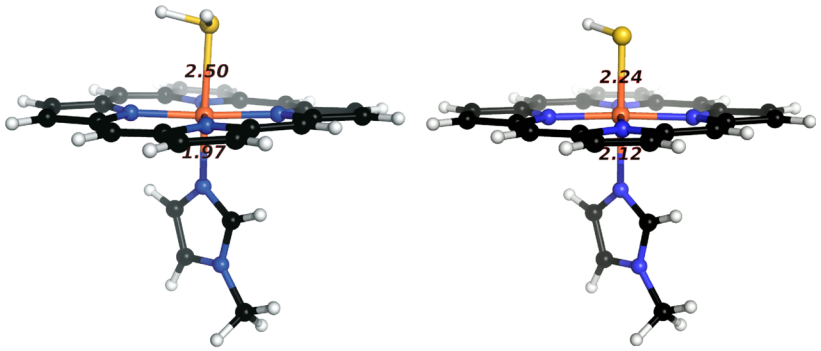

Figure 12. DFT/B3LYP-optimized models for the S = $^1/_2$ species that is formed in the reaction of Fe^{III}-Mb with sulfide. Models [**1**-H^+] and [**1**] differ with respect to the protonation state of the axial sulfur ligand. Relevant bond distances are provided in Å units.

$^5/_2$ model is predicted to be 116 kJ/mol (28 kcal/mol) higher in energy than the corresponding S = $^1/_2$ model. Although our models do not include the protein environment, it is unlikely that outer-sphere residues can collectively suppress the energy of the S = $^5/_2$ state by more than 100 kJ/mol relative to the S = $^1/_2$ state. Based on these considerations, intermediate [**1**] is described as a low-spin Fe^{III}-$^-$SH complex, consistent with our EPR data (Figure 4), though the small amount of unpaired spin density on the S atom reflects a minor contribution from the Fe^{II}-$^•$SH resonance structure.

Following formation of [**1**], addition of a sulfide anion is postulated to give the ferrous iron-bound hydro disulfide anion (Figure 11, [**2**]). Capture of a putative ([Mb(Fe−S_2H_2)] species by cryo-MS (Figure 10) provides support for the intermediacy of [**2**] or some tautomeric form. Cryo-MS detected the presence of ([Mb(Fe-(SO_3H)$^-$], an intermediate that is not predicted in our reaction mechanism. We note, however, that Figure 11 represents a minimal mechanistic scheme for myoglobin-catalyzed conversion of sulfide to thiosulfate and metal-bound hydropolysulfides. Reactive oxygen species are byproducts of the postulated reaction scheme and could very well lead to additional oxidation products as detected by cryo-MS. Furthermore, we do not have a method for evaluating whether the internal sulfurs in a catenated hydropolysulfide chain are further oxidized. The lability of the iron-bound compounds makes their handling and identification very challenging. The subsequent oxidation of intermediate [**2**] along the thiosulfate and hydropolysulfide paths to generate species [**3**] and [**4**], respectively (Figures 11), is chemically challenging, and there is insufficient information at this time on the identity of intermediates that are involved. We also do not know what intermediates build up during catalytic sulfide oxidation although the resonance Raman data indicate the dominance of one or more high spin ferrous species (Figure 5). The chemistry of sulfide oxidation by myoglobin is similar to that of human hemoglobin,[10] and is precedented in the bacterial leaching of metal sulfides by a catalytic ferric ion.[61]

An alternative mechanism for sulfide oxidation by hemoglobin was proposed recently, based on the questionable premise that sulfide binding to the heme iron is strictly O_2 dependent.[62] This observation is in direct contrast to the demonstrated stoichiometric binding of sulfide to ferric heme in hemoglobin[10] and myoglobin (Figure 2D) under strictly anaerobic conditions, the binding of sulfide to microperoxidase[50] and to a hemoglobin model,[43] both in the absence of O_2. The authors of the recent study used protocatechuate dioxygenase to scrub O_2.[62] However, the dioxygenase consumes H_2S in the presence of O_2 and protocatechuate (Yadav and Banerjee, unpublished observation), depleting H_2S, which could potentially explain the discrepant result.

A stable Fe^{III}-$^-$SH species was formed when a hemoglobin model compound was exposed to H_2S under anaerobic conditions at neutral pH.[43] In the presence of O_2, the sulfide ligand was exchanged indicating homolysis of the Fe^{III}−S bond (eq 2). Analogous ligand exchange chemistry is not observed with myoglobin during the time scale of our experiments. Furthermore,

$$Fe^{III} - {}^{-}SH + O_2 \rightarrow Fe^{II}{-}O_2 + HS^{\bullet} \quad (2)$$

$$Fe^{II}{-}O_2 + HS^{-} \rightarrow Fe^{III} - {}^{-}SH + O_2{}^{\bullet -} \quad (3)$$

unlike the Fe^{II}−O_2 complex in the model compound, which was found to undergo spontaneous ligand exchange with sulfide (eq 3),[43] neither oxy-Mb (not shown) nor oxy-Hb[10] exhibits similar reactivity with sulfide. H_2S also reduces ferric heme in cytochrome c oxidase and in cytochrome c.[63] Hence, the protein environments in myoglobin and hemoglobin modulate iron reactivity and promote oxidation of the iron-bound sulfide to more complex products, thiosulfate and hydropolysulfides.

The physiological relevance of myoglobin-dependent sulfide sequestration and/or oxidation is an interesting problem that warrants further investigation. One setting in which this chemistry might be important is in ethylmalonic encephalopathy, a disease caused by defects in the mitochondrial persulfide dioxygenase (ETHE1, which is involved in the sulfide oxidation pathway) that leads to the accumulation of H_2S. These patients display an unusual and unexplained susceptibility of cytochrome c oxidase to H_2S toxicity in muscle and brain. We speculate that myoglobin plays a role in the clinical manifestation of ethylmalonic encephalopathy by concentrating sulfide in muscle, which increases the susceptibility of cytochrome c oxidase to inhibition. Chronic inhibition of the oxidase has been shown to result in degradation of its subunits.[64] Muscle sulfide levels increase >100-fold in a mouse model of ETHE1 deficiency.[26] Tissue specific ablation of ETHE1 in murine liver, brain, and muscle successfully recapitulates the sensitivity of only the latter two tissues to selective cytochrome c oxidase deficiency.[64] Since H_2S readily traverses membranes,[65] it is probable that sulfide stored in myoglobin would be accessible to mitochondria. The slow

DOI: 10.1021/jacs.6b03456
J. Am. Chem. Soc. 2016, 138, 8476−8488

kinetics of oxidation of myoglobin-bound sulfide might set up an alternate role for it as a sulfide carrier.

CONCLUSIONS

We demonstrate that the capacity for H_2S oxidation to thiosulfate and hydropolysulfides extends beyond hemoglobin to myoglobin. Using cryo-MS, we have captured, for the first time, novel iron-bound intermediates that are formed during heme-dependent H_2S oxidation including the labile iron-bound hydrodisulfide species that is proposed to be at the branch point where the pathways for thiosulfate and hydropolysulfide formation bifurcate. Resonance Raman, EPR, and XAS data complemented by DFT calculations provide additional support for a key early intermediate in this noncanonical H_2S oxidation pathway. We speculate that the combination of relatively rapid H_2S binding and slow oxidation contributes to targeted inhibition of cytochrome c oxidase in muscle in ETHE1 deficiency, a condition in which the canonical sulfide oxidation pathway is impaired.

AUTHOR INFORMATION

Corresponding Author

*rbanerje@umich.edu

Author Contributions

#T.B. and V.V. contributed equally.

Notes

The authors declare no competing financial interest.

ACKNOWLEDGMENTS

This work was supported in part by grants from the National Institutes of Health (GM112455 to R.B. and DK068139 to T.L.S.) and the American Heart Association (14POST18760003 to P.K.Y.). We thank Dr. Markus Ruetz for help with the EPR studies, Andrew Hunt for help with the resonance Raman studies, and Dr. David Ballou for his assistance with the O_2 consumption assays.

REFERENCES

(1) Kabil, O.; Banerjee, R. *J. Biol. Chem.* **2010**, *285*, 21903.
(2) Kimura, H. *Antioxid. Redox Signaling* **2015**, *22*, 347.
(3) Hill, B. C.; Woon, T. C.; Nicholls, P.; Peterson, J.; Greenwood, C.; Thomson, A. J. *Biochem. J.* **1984**, *224*, 591.
(4) Kabil, O.; Banerjee, R. *Antioxid. Redox Signaling* **2014**, *20*, 770.
(5) Mustafa, A. K.; Gadalla, M. M.; Sen, N.; Kim, S.; Mu, W.; Gazi, S. K.; Barrow, R. K.; Yang, G.; Wang, R.; Snyder, S. H. *Sci. Signaling* **2009**, *2*, ra72.
(6) Mishanina, T. V.; Libiad, M.; Banerjee, R. *Nat. Chem. Biol.* **2015**, *11*, 457.
(7) Roman-Morales, E.; Pietri, R.; Ramos-Santana, B.; Vinogradov, S. N.; Lewis-Ballester, A.; Lopez-Garriga, J. *Biochem. Biophys. Res. Commun.* **2010**, *400*, 489.
(8) Nakamura, S.; Nakamura, M.; Yamazaki, I.; Morrison, M. *J. Biol. Chem.* **1984**, *259*, 7080.
(9) Nicholls, P. *Biochem. J.* **1961**, *81*, 374.
(10) Vitvitsky, V.; Yadav, P. K.; Kurthen, A.; Banerjee, R. *J. Biol. Chem.* **2015**, *290*, 8310.
(11) Hildebrandt, T. M.; Grieshaber, M. K. *FEBS J.* **2008**, *275*, 3352.
(12) Yong, R.; Searcy, D. G. *Comp. Biochem. Physiol., Part B: Biochem. Mol. Biol.* **2001**, *129*, 129.
(13) Kendrew, J. C.; Bodo, G.; Dintzis, H. M.; Parrish, R. G.; Wyckoff, H.; Phillips, D. C. *Nature* **1958**, *181*, 662.
(14) Garry, D. J.; Ordway, G. A.; Lorenz, J. N.; Radford, N. B.; Chin, E. R.; Grange, R. W.; Bassel-Duby, R.; Williams, R. S. *Nature* **1998**, *395*, 905.
(15) Flogel, U.; Merx, M. W.; Godecke, A.; Decking, U. K.; Schrader, J. *Proc. Natl. Acad. Sci. U. S. A.* **2001**, *98*, 735.
(16) Hendgen-Cotta, U. B.; Merx, M. W.; Shiva, S.; Schmitz, J.; Becher, S.; Klare, J. P.; Steinhoff, H. J.; Goedecke, A.; Schrader, J.; Gladwin, M. T.; Kelm, M.; Rassaf, T. *Proc. Natl. Acad. Sci. U. S. A.* **2008**, *105*, 10256.
(17) Rassaf, T.; Flogel, U.; Drexhage, C.; Hendgen-Cotta, U.; Kelm, M.; Schrader, J. *Circ. Res.* **2007**, *100*, 1749.
(18) Kreutzer, U.; Jue, T. *Am. J. Physiol. Heart Circ. Physiol.* **2003**, *286*, 985H.
(19) Eich, R. F.; Li, T.; Lemon, D. D.; Doherty, D. H.; Curry, S. R.; Aitken, J. F.; Mathews, A. J.; Johnson, K. A.; Smith, R. D.; Phillips, G. N., Jr.; Olson, J. S. *Biochemistry* **1996**, *35*, 6976.
(20) Shintani, T.; Iwabuchi, T.; Soga, T.; Kato, Y.; Yamamoto, T.; Takano, N.; Hishiki, T.; Ueno, Y.; Ikeda, S.; Sakuragawa, T.; Ishikawa, K.; Goda, N.; Kitagawa, Y.; Kajimura, M.; Matsumoto, K.; Suematsu, M. *Hepatology* **2009**, *49*, 141.
(21) Livingston, D. J.; McLachlan, S. J.; La Mar, G. N.; Brown, W. D. *J. Biol. Chem.* **1985**, *260*, 15699.
(22) Kraus, D. W.; Wittenberg, J. B.; Jing-Fen, L.; Peisach, J. *J. Biol. Chem.* **1990**, *265*, 16054.
(23) Strianese, M.; De Martino, F.; Pellecchia, C.; Ruggiero, G.; D'Auria, S. *Protein Pept. Lett.* **2011**, *18*, 282.
(24) Libardi, S. H.; Pindstrup, H.; Cardoso, D. R.; Skibsted, L. H. *J. Agric. Food Chem.* **2013**, *61*, 2883.
(25) Tiranti, V.; D'Adamo, P.; Briem, E.; Ferrari, G.; Mineri, R.; Lamantea, E.; Mandel, H.; Balestri, P.; Garcia-Silva, M. T.; Vollmer, B.; Rinaldo, P.; Hahn, S. H.; Leonard, J.; Rahman, S.; Dionisi-Vici, C.; Garavaglia, B.; Gasparini, P.; Zeviani, M. *Am. J. Hum. Genet.* **2004**, *74*, 239.
(26) Tiranti, V.; Viscomi, C.; Hildebrandt, T.; Di Meo, I.; Mineri, R.; Tiveron, C.; Levitt, M. D.; Prelle, A.; Fagiolari, G.; Rimoldi, M.; Zeviani, M. *Nat. Med.* **2009**, *15*, 200.
(27) Zhu, W.; Lin, A.; Banerjee, R. *Biochemistry* **2008**, *47*, 6226.
(28) Yadav, P. K.; Martinov, M.; Vitvitsky, V.; Seravalli, J.; Wedmann, R.; Filipovic, M. R.; Banerjee, R. *J. Am. Chem. Soc.* **2016**, *138*, 289.
(29) Wood, J. L. *Methods Enzymol.* **1987**, *143*, 25.
(30) Jiang, Z. Y.; Woollard, A. C.; Wolff, S. P. *FEBS Lett.* **1990**, *268*, 69.
(31) George, G. N.; George, S. J.; Bommannavar, A. S. *EXAFSPAK* (2001); http://ssrl.slac.stanford.edu/exafspak.html.
(32) Cook, J. D.; Bencze, K. Z.; Jankovic, A. D.; Crater, A. K.; Busch, C. N.; Bradley, P. B.; Stemmler, A. J.; Spaller, M. R.; Stemmler, T. L. *Biochemistry* **2006**, *45*, 7767.
(33) Cotelesage, J. J.; Pushie, M. J.; Grochulski, P.; Pickering, I. J.; George, G. N. *J. Inorg. Biochem.* **2012**, *115*, 127.
(34) Neese, F. https://orcaforum.cec.mpg.de/, 2015.
(35) Schäfer, A.; Horn, H.; Ahlrichs, R. *J. Chem. Phys.* **1992**, *97*, 2571.
(36) Schäfer, A.; Huber, C.; Ahlrichs, R. *J. Chem. Phys.* **1994**, *100*, 5829.
(37) Becke, A. D. *J. Chem. Phys.* **1986**, *84*, 4524.
(38) Perdew, J. P. 1986, *33*, 8822.
(39) Becke, A. D. *J. Chem. Phys.* **1993**, *98*, 5648.
(40) Lee, C.; Yang, W.; Parr, R. G. *Phys. Rev. B: Condens. Matter Mater. Phys.* **1988**, *37*, 785.
(41) *The PyMOL Molecular Graphics System*, version 1.7.6 ed.; Schrödinger, LLC.
(42) Nicoletti, F. P.; Comandini, A.; Bonamore, A.; Boechi, L.; Boubeta, F. M.; Feis, A.; Smulevich, G.; Boffi, A. *Biochemistry* **2010**, *49*, 2269.
(43) Watanabe, K.; Suzuki, T.; Kitagishi, H.; Kano, K. *Chem. Commun. (Cambridge, U. K.)* **2015**, *51*, 4059.
(44) Brittain, T.; Yosaatmadja, Y.; Henty, K. *IUBMB Life* **2008**, *60*, 135.
(45) Ida, T.; Sawa, T.; Ihara, H.; Tsuchiya, Y.; Watanabe, Y.; Kumagai, Y.; Suematsu, M.; Motohashi, H.; Fujii, S.; Matsunaga, T.; Yamamoto, M.; Ono, K.; Devarie-Baez, N. O.; Xian, M.; Fukuto, J. M.; Akaike, T. *Proc. Natl. Acad. Sci. U. S. A.* **2014**, *111*, 7606.

DOI: 10.1021/jacs.6b03456
J. Am. Chem. Soc. 2016, 138, 8476−8488

(46) Kraus, D. W.; Wittenberg, J. B.; Lu, J. F.; Peisach, J. *J. Biol. Chem.* **1990**, *265*, 16054.
(47) Berzofsky, J. A.; Peisach, J.; Blumberg, W. E. *J. Biol. Chem.* **1971**, *246*, 3367.
(48) Jeyarajah, S.; Proniewicz, L. M.; Bronder, H.; Kincaid, J. R. *J. Biol. Chem.* **1994**, *269*, 31047.
(49) Spiro, T. G.; Burke, J. M. *J. Am. Chem. Soc.* **1976**, *98*, 5482.
(50) Bieza, S. A.; Boubeta, F.; Feis, A.; Smulevich, G.; Estrin, D. A.; Boechi, L.; Bari, S. E. *Inorg. Chem.* **2015**, *54*, 527.
(51) Cerda, J.; Echevarria, Y.; Morales, E.; Lopez-Garriga, J. *Biospectroscopy* **1999**, *5*, 289.
(52) Westre, T. E.; Kennepohl, P.; DeWitt, J. G.; Hedman, B.; Hodgson, K. O.; Solomon, E. I. *J. Am. Chem. Soc.* **1997**, *119*, 6297.
(53) Wilson, S. A.; Green, E.; Mathews, II; Benfatto, M.; Hodgson, K. O.; Hedman, B.; Sarangi, R. *Proc. Natl. Acad. Sci. U. S. A.* **2013**, *110*, 16333.
(54) Yano, J.; Kern, J.; Irrgang, K. D.; Latimer, M. J.; Bergmann, U.; Glatzel, P.; Pushkar, Y.; Biesiadka, J.; Loll, B.; Sauer, K.; Messinger, J.; Zouni, A.; Yachandra, V. K. *Proc. Natl. Acad. Sci. U. S. A.* **2005**, *102*, 12047.
(55) Cramer, S. P.; Dawson, J. H.; Hodgson, K. O.; Hager, L. P. *J. Am. Chem. Soc.* **1978**, *100*, 7282.
(56) Hahn, J. E.; Hodgson, K. O.; Andersson, L. A.; Dawson, J. H. *J. Biol. Chem.* **1982**, *257*, 10934.
(57) Rios-Gonzalez, B. B.; Roman-Morales, E. M.; Pietri, R.; Lopez-Garriga, J. *J. Inorg. Biochem.* **2014**, *133*, 78.
(58) Champion, P. M.; Stallard, B. R.; Wagner, G. C.; Gunsalus, I. C. *J. Am. Chem. Soc.* **1982**, *104*, 5469.
(59) Galinato, M. G.; Spolitak, T.; Ballou, D. P.; Lehnert, N. *Biochemistry* **2011**, *50*, 1053.
(60) Green, E. L.; Taoka, S.; Banerjee, R.; Loehr, T. M. *Biochemistry* **2001**, *40*, 459.
(61) Schippers, A.; Sand, W. *Appl. Environ. Microbiol.* **1999**, *65*, 319.
(62) Spolitak, T.; Hollenberg, P. F.; Ballou, D. P. *Arch. Biochem. Biophys.* **2016**, *600*, 33.
(63) Nicholls, P.; Kim, J. K. *Can. J. Biochem.* **1982**, *60*, 613.
(64) Di Meo, I.; Fagiolari, G.; Prelle, A.; Viscomi, C.; Zeviani, M.; Tiranti, V. *Antioxid. Redox Signaling* **2011**, *15*, 353.
(65) Mathai, J. C.; Missner, A.; Kugler, P.; Saparov, S. M.; Zeidel, M. L.; Lee, J. K.; Pohl, P. *Proc. Natl. Acad. Sci. U. S. A.* **2009**, *106*, 16633.
(66) Romero, F. J.; Ordonez, I.; Arduini, A.; Cadenas, E. *J. Biol. Chem.* **1992**, *267*, 1680.

DOI: 10.1021/jacs.6b03456
J. Am. Chem. Soc. 2016, 138, 8476−8488